Journal of Power Sources 196 (2011) 2650–2660

Contents lists available at ScienceDirect

Journal of Power Sources

journal homepage: www.elsevier.com/locate/jpowsour

Performance test and degradation analysis of direct methanol fuel cell membrane electrode assembly during freeze/thaw cycles

Hou-Chin Cha*, Charn-Ying Chen, Rui-Xiang Wang, Chun-Lung Chang

Institute of Nuclear Energy Research (INER), 1000, Wenhua Rd., Chiaan Village, P.O. Box 3-14, Lungtan, Taiwan

ARTICLE INFO

Article history:
Received 8 November 2010
Accepted 8 November 2010
Available online 12 November 2010

Keywords:
Direct methanol fuel cell
Membrane electrode assembly
Subzero temperature
Polarization curve
Electrochemical impedance spectroscopy

ABSTRACT

Performance and degradation of direct methanol fuel cell (DMFC) membrane electrode assembly (MEA) are analyzed after repeated freeze/thaw cycles. Three different MEAs stored at −20 °C for 8 h with the anode side full of methanol solution are selected to test the effects of low temperatures on performance. After the cell heated to 60 °C within 30 min, they are inspected to determine the degradation mechanism. The resistance *R* obtained by the polarization curve is essential for identifying the main component affecting cell performance. The electrochemical impedance spectroscopy (EIS) technique is used to characterize the DMFC after freeze/thaw cycles. Thus, deterioration is assessed by measuring the high-frequency resistance (HFR) and the charge-transfer resistance (CTR). The electrochemical surface area (ECA) is employed to investigate not only the actual chemical degradation but also membrane status since sudden loss of ECA on the cathode side can result from a broken membrane. Moreover, a strategy is designed to simulate actual conditions that may prevent the membrane from being broken. A DMFC stack without any heating or heat-insulation devices shall avoid to be stored at subzero temperatures since the membrane will be useless due to frozen of methanol solution.

© 2010 Elsevier B.V. All rights reserved.

1. Introduction

In recent decades, direct methanol fuel cells (DMFCs) have been considered as an alternative power source because of their many advantages, including high power density, ease of fuel storage and refilling, portability and mild operating condition. However, in some cases, these devices have to be able to withstand extreme environmental conditions such as shocks, and changes in the humidity and temperature. In a proton exchange membrane fuel cell (PEMFC) system, water is produced on the cathode side due to the oxygen reduction reaction (ORR). Once the cell shuts down and is kept at subzero temperature, generally the water in the cell will freeze. Freezing may negatively impact the fuel cell materials and its components. In a DMFC system, however, the situation is even worse, not only because of the water produced by ORR on the cathode side, but also because of the aqueous solution on the anode side. Water in fuel cells will lead to ice formation in membrane, catalyst layers (CLs), gas diffusion layers (GDLs) and channels of bipolar plates. Thus, the ice will cause increasing contact resistance due to delamination of the GDL, decreasing power output due to microstructural damage of the catalyst layer, and, most importantly, formation of cracks and pinholes that can induce unrecoverable performance loss.

Until now, many studies have analyzed the degradation mechanisms in PEMFC stacks under subzero conditions such as cold startup with hydrogen pump at subzero temperatures. The effects of subzero temperatures on fuel cell performance during cold startup have also been studied [1–8]. However, few studies have analyzed DMFC. Up to now, only two articles corresponding to the subzero temperatures issues have been published. Krewer et al. investigated performance change in MEAs of DMFC caused by storage at −10 °C and 60 °C under different experimental conditions. The article was focusing on possible damage and deactivation of the MEA during storage [9]. Park et al. studied cold startup and operation of a DMFC at subzero temperatures by using a 10-cell stack. From the results, self-heating operation of DMFC stacks without any heating or heat-insulation devices appeared to be limited around −10 °C. A successful self-heating startup of DMFC without heating device, even considering the performance loss, was believed to be achieved at even lower temperature in this study [10].

A frequently used method to probe interfacial processes and speciation in electrochemical systems is electrochemical impedance spectroscopy (EIS). The EIS reveals characteristics such as high-frequency resistance (HFR), which is the sum of the membrane, electrodes, contacts, and other resistances, and charge-transfer resistance (CTR), which is mass transportation capability.

* Corresponding author. Tel.: +886 3 4711400x2960; fax: +886 3 4711409.
E-mail address: hccha@iner.gov.tw (H.-C. Cha).

0378-7753/$ – see front matter © 2010 Elsevier B.V. All rights reserved.
doi:10.1016/j.jpowsour.2010.11.054

The EIS studies of DMFCs under various test conditions, such as a large electrode area, high temperature, and large DC current, have been recently performed [11–18]. A previous work by the authors was the first to use an Ag/AgCl electrode as a reference electrode with minimal instability to observe the impedance of each electrode [19,20]. The unique advantages of this reference electrode are that it can avoid the effect of impurities such as O_2 and can be easily applied in the electrochemical system. This extended method can simultaneously determine the EIS response and polarization curve of the individual anode, individual cathode, and individual membrane for various operating conditions.

This work explores the degradation mechanism of cell components during freeze/thaw cycles. The performance data and EIS measurements were compared between fresh and post-mortem MEAs. Also, the electrochemical surface areas (ECAs) measured by cyclic voltammetry (CV) in the anode and cathode catalysts were evaluated by hydrogen-desorption to identify microstructural change as well as chemical degradation. To understand the correlation between cell performance and freeze/thaw cycles, the extended method, which separates the individual anode, individual cathode and individual membrane, is applied to clarify where the real problem is. Finally, a simulation of actual condition was performed to evaluate a strategy for reducing decay rate.

2. Experimental

2.1. MEA preparation or fabrication

Three types of MEAs were taken into consideration for DMFC performance test to verify the quality after freeze/thaw cycles. The MEA 1, a commercial product made of Nafion 117 membrane, was a five layers structure (GDL/CL/membrane/CL/GDL). The catalyst-coated membrane (CCM), which the anode and cathode catalysts were PtRu (1:1 atomic ratio) and Pt, and the catalyst loading was 2 mg cm^{-2} on each side, was embedded in a pair of GDLs. The material used for GDLs on both the anode and cathode sides was carbon paper, and uncertain amount of catalyst was discovered in the micro-porous layer (MPL) on the anode side. The MEA 2, a commercial product made of Nafion 117 membrane, was a three layers structure (CL/membrane/CL). The anode and cathode catalysts were PtRu and Pt, and the catalyst loading was 2 mg cm^{-2} on each side. The fresh MEA was initially conserved in deionized water to maintain its humidity. The materials used for GDLs on the anode and cathode sides were carbon paper (SGL) and carbon cloth (BASF), respectively. The MEA 3, an in-house product made of Nafion 117 membrane, was also a three layers structure (CL/membrane/CL). After Nafion 117 membrane was cleansed by boiling in deionized water, 3 wt.% H_2O_2, 3 wt.% H_2SO_4, deionized water and deionized water again for 1 h in each step, a thin layer of electrode was coated on each surface of the membrane by screen printing with the prepared catalysts. The catalysts were purchased from Johnson Matthey Inc. The electrode ink was fabricated from a mixture of Pt–Ru/C or Pt/C catalysts with a Nafion solution (DuPont). Catalysts of 40 wt.%Pt–20 wt.%Ru (anode) and 60 wt.%Pt (cathode) were supported on a conductive carbon black with a high surface area. The MEA was then obtained by hot pressing at 120 °C and 5–30 kg cm^{-2} for 1–2 min with the same catalyst loading of about 3.5–3.85 mg cm^{-2} in each electrode [21–25]. The GDL used for the MEA 3 was the same with the MEA 2. The active areas of all MEAs were 25 cm^2, and the gasket thickness of both the anode and cathode sides were 0.2 mm. The MEA was installed into a test block which made of a pair of stainless steel-plated current collectors. A serpentine-serpentine flow field was machined in the plates with parallel geometry (1 mm wide, 1.2 mm deep, with ridges 1 mm high).

2.2. Single-cell operation

Before the single-cell operating, a 3 wt.% methanol solution was fed from a methanol solution container with a pump and preheated to the operating temperature at 60 °C. During the DMFC performance test, following steps were sequentially operated to complete a single freeze/thaw cycle.

(i) Constant current mode: a constant current of 3 A was applied to the cell for 30 min to keep the cell performance stable.
(ii) Polarization measurement: the stoichiometric flow rate of the anode was set to 6 when a 3 wt.% methanol solution was used at 60 °C, and the stoichiometric flow rate of the cathode was also set to 6. The range of measured voltages was set from 0.8 V to 0.2 V with 0.05 V per interval drop.
(iii) EIS measurement: for all impedance measurements, the range of measured frequencies was set from 1 kHz to 0.05 Hz with 10 steps per logarithmic decade. The stoichiometric flow rate of both the anode and the cathode were set to 6, and a constant current of 5 A was applied for entire measurement.
(iv) ECA measurement: for anodic ECA test, the cathode served as a dynamic hydrogen electrode (DHE), was fed with humidified hydrogen at 20 ml min^{-1}. The anode was fed with humidified nitrogen at 300 ml min^{-1}. On the contrary, for cathodic ECA test, the anode served as a DHE, was fed with humidified hydrogen at 20 ml min^{-1}. The cathode was fed with humidified nitrogen at 300 ml min^{-1}. The potential was then scanned from 0 to 0.8 V at a scan rate of 20 mV s^{-1}, both in anode and cathode side.
(v) Freeze mode: the DMFC test block was placed in the programmable temperature and humidity chamber to maintain the freezing condition for 8 h.
(vi) Rapidly thaw mode: after the freeze mode, the chamber was heated up to 60 °C in 30 min to make the ice inside the test block thawing.

2.3. Characterization of MEA

Testing was performed by a computer-controlled Medusa RD Fuel Cell Test Station (Teledyne Energy Systems, Inc.) with a 50 A/100 W Model 890CL electronic load (Scribner Associates, Inc.) and Model 880 Frequency Response Analyzer (Scribner Associates, Inc.). To resolve the anode and cathode impedance, an Ag/AgCl electrode (MF-2052, BAS Inc.) was placed at the region of constant potential (RCP) [19,21,26] of the membrane as reference electrode. For measurement of the half-cell impedance of the anode, the cathode electrode was operated as a DHE. Clearly, the real HFR of the anode can be isolated by using the Ag/AgCl. Furthermore, the CTR of each electrode, as well as the individual HFR, were separated during operation of the different airflows of 100 and 300 ml min^{-1}. The detailed description of the setup of reference electrode was proposed and demonstrated in our previous work [19]. All the impedance spectra were measured under the galvanostatic mode.

The ECA of the catalyst measured by CV experiments was performed by a ZAHNER IM6/6eX system. The ECAs of catalysts were evaluated by using hydrogen-desorption method. The reaction of interest was the electrochemical reduction of protons (H^+) and subsequent deposition of atomic hydrogen on the surface of the Pt catalyst, $Pt + H^+ + e^- \leftrightarrow Pt - H_{ads}$. The atomic hydrogen adsorption charge density due to this reaction could be determined from the CV scan. The ECA of the Pt catalyst [27] was calculated from the charge density, the well-established quantity for the charge to reduce a monolayer of protons on Pt.

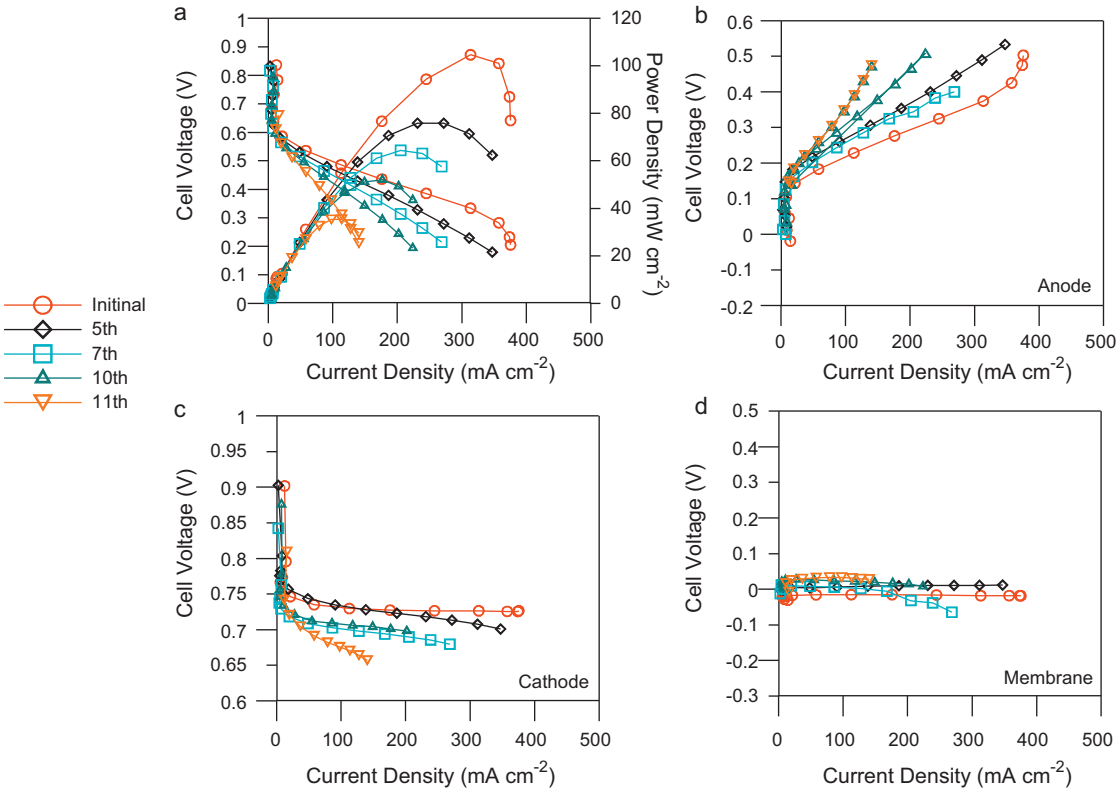

Fig. 1. Polarization curves of the MEA 1 during the freeze/thaw cycling. (a) Full-cell, (b) anode, (c) cathode, and (d) membrane. Cell temperature is 60 °C, both the anode and cathode flow are 6-stoichiometry.

3. Results and discussion

3.1. Performance test of the MEA 1

Fig. 1 shows the polarization curves associated with the individual anode, cathode, and membrane performance of the MEA 1. Since the performance was similar during the initial state to the 4th test, thus, only the initial polarization curve was drawn. Fig. 1(a) shows that the fresh MEA performed better than the post-mortem MEA did. Although performance did not significantly change during the first 4 freeze/thaw cycles, performance gradually decreased as the number of freeze/thaw cycle increased. Fig. 1(b) shows the individual anode polarization curve. The $|\Delta V/\Delta I|$ values corresponding to the resistance R in the first 9 freeze/thaw cycles were almost the same, but the 10th freeze/thaw cycle exhibited an ascending trend. The increase was even larger in the 11th freeze/thaw cycle. The increasing $|\Delta V/\Delta I|$ values may have resulted from microstructural changes damaging the membrane and catalyst layer and delaminating the GDL. Fig. 1(c) shows the individual cathode polarization curve. The $|\Delta V/\Delta I|$ values in the first 10 freeze/thaw cycles were similar, but the 11th freeze/thaw cycle exhibited an ascending trend. Fig. 1(d) shows the individual membrane polarization curve. The $|\Delta V/\Delta I|$ values did not significantly change throughout the entire freeze/thaw cycle, which implied that the membrane was not the main determinant of the polarization curve. Comparison of the individual anode, cathode and membrane polarization curves showed that performance loss was greater on the anode side during the freeze/thaw cycles.

Fig. 2 shows the electrochemical behavior of the MEA 1. The 11th EIS measurement is not shown due to the dramatic degradation of the MEA 1, thus; only the first 10 data are recorded. In Fig. 2(a), the effect of both the anode and the cathode on the overall reaction is plotted as a full-cell impedance spectrum. The HFR corresponding to the ohmic resistance of cell elements was the sum of resistances such as the membrane, electrodes, contacts, and other components. The HFR of the full-cell impedance spectrum presented an increasing trend with ascending freeze/thaw cycles, thus, freezing might negatively affect the contact resistance. The CTR also correlated with the number of freeze/thaw cycles. In the initial state, the CTR of the full-cell spectrum showed a small arc when the MEA 1 was in a normal condition. As the number of freeze/thaw cycles increased, the diameter of the arc increased and the arc became irregular in the low-frequency region. The causes of the change in CTR spectra were revealed by the individual anode, cathode, and membrane impedance spectra. Fig. 2(b) presents the CTR spectrum of the individual anode. The double arcs may have resulted from different ORR paths reflecting different MEA components. The first arc corresponding to the higher frequency region exhibited the mass-diffusion phenomenon in the ORR of the anode catalyst layer whereas the second arc corresponding to the lower frequency region exhibited the mass-diffusion phenomenon observed in the ORR of the other components, such as the catalyst coated on the MPL [20]. The double arcs both became larger or even diverged as the number of freeze/thaw cycles increased, which indicated that the diffusion problem began to hinder mass transport during the freeze/thaw cycles. Fig. 2(c) plots the CTR spectrum of the individual cathode. The arcs also became larger as the number of freeze/thaw cycles increased but were not divergent, and the increase was relatively smaller on the cathode side than on the anode side. Thus, the results might exhibit that the diffusion was less problematic on the cathode side than on the anode side. Fig. 2(d) plots the CTR spectrum of the individual membrane. Since the CTR spectra were similar, i.e., the membrane was not the dominant influence on cell performance. The ECA of catalyst could be estimated by analyzing the integration of hydrogen desorption/adsorption peaks obtained in forward and reverse

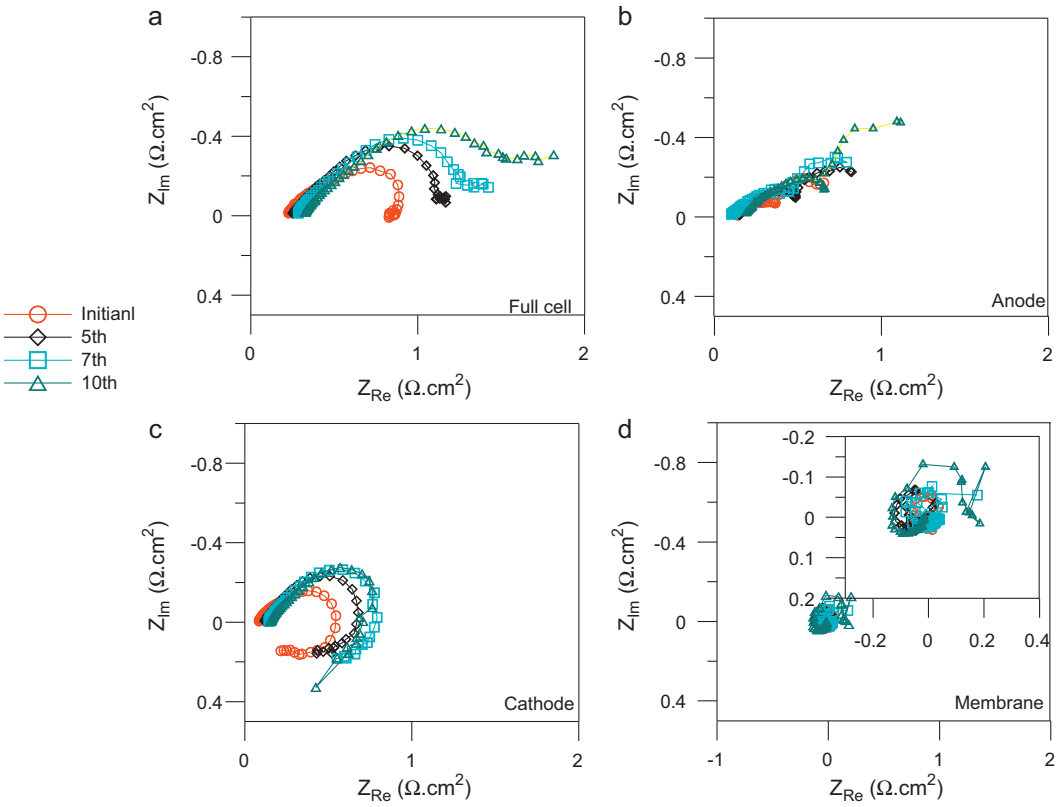

Fig. 2. EIS measurement results of the MEA 1 during the freeze/thaw cycling. (a) Full-cell, (b) anode, (c) cathode, and (d) membrane. Cell temperature is 60 °C, both the anode and cathode flow are 6-stoichiometry.

scans, respectively. Fig. 3 shows the CV testing results obtained by hydrogen-desorption method. The ECA loss estimated not only the microstructural change such as catalyst agglomeration and growth but also chemical degradation caused by poisoning of catalysts. After the 10th freeze/thawing cycle, the ECA values of MEA 1 decreased 15.7% and 7.4% in the anode and cathode catalysts, respectively. The tolerance for measurement error was 10%, thus, the ECA loss was less dramatic. However, after the 11th freeze/thaw cycle, the ECA values of MEA 1 decreased 16.5% and 30.4% in the anode and cathode catalysts, respectively. The dramatic ECA loss on the cathode side may have been attributable to the crossover problem due to abrupt breakage of the membrane.

In summary, the $|\Delta V/\Delta I|$ value associated with the resistance R in polarization curves gradually increased as the number of freeze/thaw cycles increased on both the anode and the cathode side. However, the slope of the $|\Delta V/\Delta I|$ was larger on the anode side. This outcome was consistent with EIS measurements. Although the CTRs of the full-cell, individual anode, and individual cathode were all amplified, the change on the anode side was clearly the determining factor. Besides, the HFRs of the full-cell, individual anode, and individual cathode all gradually increased, which implied that the increase of contact resistance due to assembly problem may affect any MEA 1 component. The ECA measurement showed similar results as all the changes were in the acceptable range until the dramatic degradation that occurred after the 11th freeze/thaw cycle. Apparently, the HFR change caused by delamination of the catalyst layers and GDL and the CTR change caused by diffusion hindrance on the anode side were the major causes of degraded cell performance after freeze/thaw cycles. Nevertheless, as mentioned before, the abrupt performance degradation was clearly caused by crossover resulting in ECA loss.

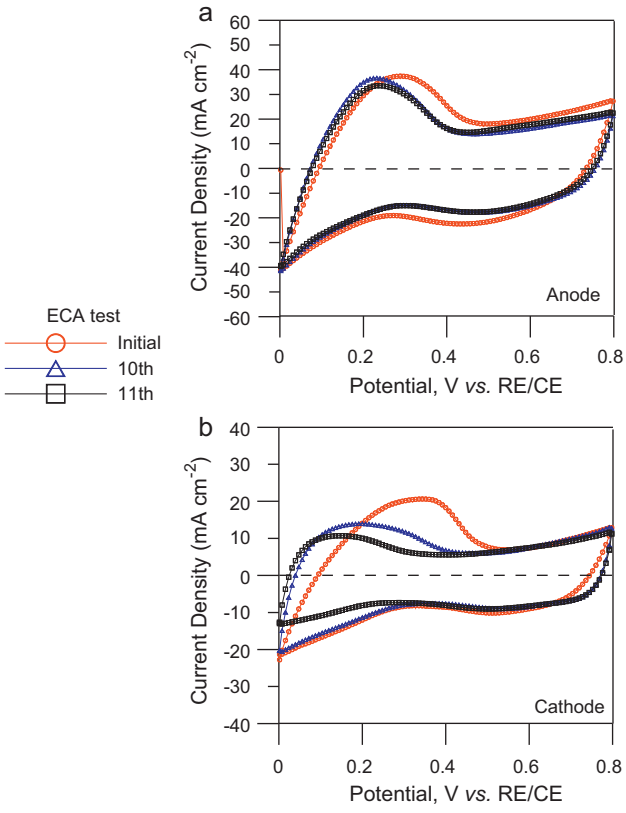

Fig. 3. Electrochemical areas (ECAs) of the catalysts on MEA 1 evaluated by hydrogen-desorption test: (a) anode catalysts and (b) cathode catalysts.

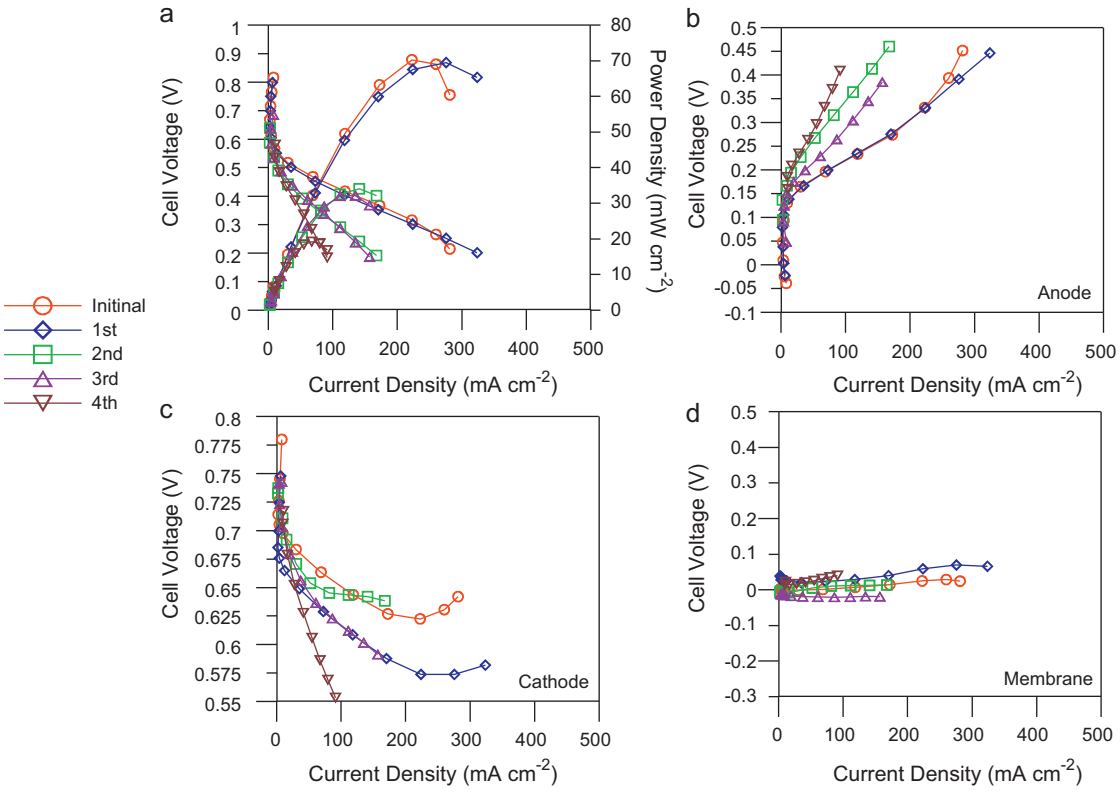

Fig. 4. Polarization curves of the MEA 2 during the freeze/thaw cycling. (a) Full-cell, (b) anode, (c) cathode, and (d) membrane. Cell temperature is 60 °C, both the anode and cathode flow are 6-stoichiometry.

3.2. Performance test of the MEA 2

Fig. 4 shows the polarization curves associated with the individual anode, cathode, and membrane performance of the MEA 2. In Fig. 4(a), peak power density of the MEA 2 decreased dramatically after the 2nd freeze/thaw cycle and the performance loss was estimated to be 50%. Moreover, the performance loss after the 4th freeze/thaw cycle increased to 80%. Fig. 4(b) shows the individual anode polarization curve. The $|\Delta V/\Delta I|$ values exhibited an increasing trend after the 2nd freeze/thaw cycle and increased dramatically after the 4th freeze/thaw cycle. Fig. 4(c) shows the individual cathode polarization curve. Like the tendency performed on the anode side, the $|\Delta V/\Delta I|$ values on the cathode side also increased dramatically after the 4th freeze/thaw cycle. Fig. 4(d) shows the individual membrane polarization curve. The $|\Delta V/\Delta I|$ values did not significantly change throughout the entire freeze/thaw cycles, which implied that the membrane was not the main determinant of the polarization curve. Comparison of the individual anode, cathode and membrane polarization curves showed that the $|\Delta V/\Delta I|$ value was larger on the anode side, which implied that performance loss was greater on the anode side during the freeze/thaw cycles.

Fig. 5 shows the electrochemical behavior of the MEA 2. The 4th EIS measurement is not shown due to the dramatic degradation of the MEA 2, thus; only the first 3 data are recorded. Fig. 5(a) plots the full-cell spectrum. The HFR of the full-cell impedance spectrum showed no significant change after the freeze/thaw cycles. Thus, the ohmic resistance of cell elements was fixed which exhibited that the MEA 2 was kept compact between the membrane, electrodes, GDLs, and other contacts. But, the CTR increased after the 2nd freeze/thaw cycle. In the initial state, the CTR of the full-cell spectrum showed a small arc when the MEA 2 was in a normal condition. As the number of freeze/thaw cycles increased, the diameter of the arc increased and the arc became irregular in the low-frequency region. The causes of the change in CTR spectra were revealed by the individual anode, cathode, and membrane spectra. Fig. 5(b) presents the CTR spectrum of the individual anode. The arc became larger and diverged after the 2nd freeze/thaw cycle. Fig. 5(c) presents the CTR spectrum of the individual cathode. The arc became larger after the 2nd freeze/thaw cycle, and even diverged after the 3rd freeze/thaw cycle. Obviously, the increase of CTR on the anode side was larger, thus, mass transport problem on the anode side was more serious. Fig. 5(d) plots the CTR spectrum of the individual membrane. Since the spectra were similar, i.e., the membrane was not the dominant influence on cell performance. Also, the ECA values of MEA 2 shown in Fig. 6 were calculated after the freeze/thaw cycles, and the values decreased 14.8% and 41.3% in the anode and cathode catalysts, respectively. It was noted that, after the 2nd freeze/thaw cycle, a little amount of methanol solution was observed on the cathode side while the test block was heated at the rapidly thaw mode. Therefore, some pinholes were formed in the membrane, and the methanol solution could reach and poison the catalyst on the cathode side.

In summary, the $|\Delta V/\Delta I|$ value associated with the resistance R in polarization curves gradually increased as the number of freeze/thaw cycles increased on both the anode and the cathode side. That was in agreement with EIS measurements. The CTR spectrum of the anode was even irregular and divergent might result from the formation of pinholes in the membrane. While the polarization curve and EIS measurement were testing, the pressure in cathode side was higher than in anode side; thus, the methanol solution was compressed by the penetrated air from the cathode side. The CTR spectra revealed that the methanol solution diffused laboriously on the anode side, which might result from any transport problem. From the ECA measurements, methanol crossover was obviously the major factor to poison the catalyst on the cath-

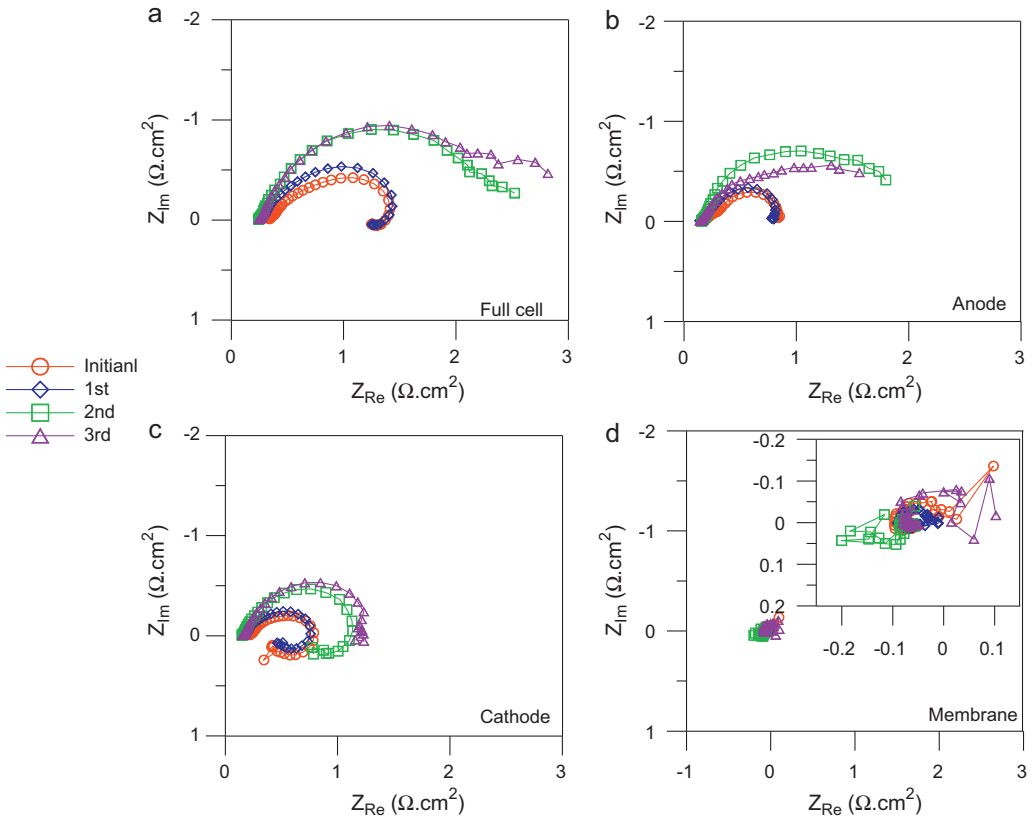

Fig. 5. EIS measurement results of the MEA 2 during the freeze/thaw cycling. (a) Full-cell, (b) anode, (c) cathode, and (d) membrane. Cell temperature is 60 °C, both the anode and cathode flow are 6-stoichiometry.

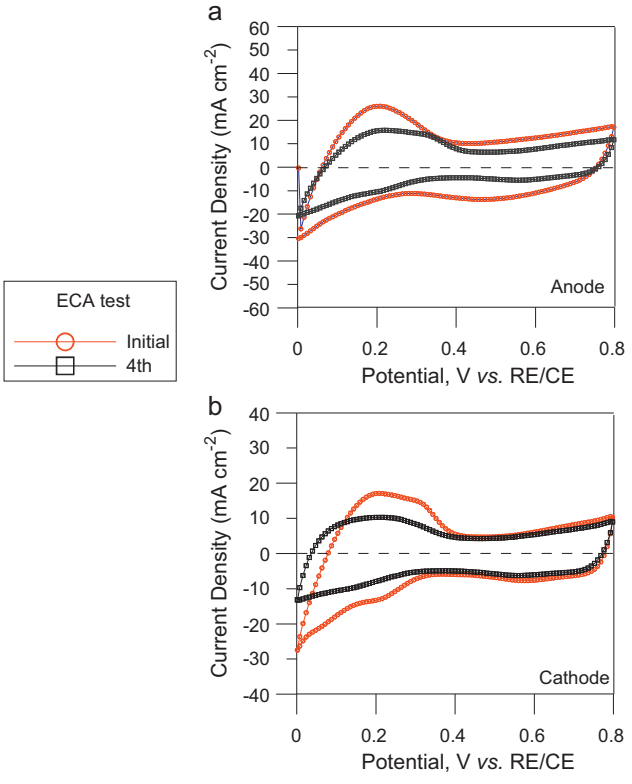

Fig. 6. Electrochemical areas (ECAs) of the catalysts on MEA 2 evaluated by hydrogen-desorption test: (a) anode catalysts and (b) cathode catalysts.

ode side, and that would lead to tremendous performance loss. Besides, the membrane was broken (a huge area of hole formed) after freeze/thaw cycles implied that the MEA 2 could not overcome the repeated stress change.

3.3. *Performance test of the MEA 3*

Fig. 7 shows the polarization curves associated with the individual anode, cathode, and membrane performance of the MEA 3. In Fig. 7(a), although performance did not significantly change before the 8th freeze/thaw cycle, performance gradually decreased after the 8th freeze/thaw cycle. Besides, the peak power density decreased 35% after the 11th freeze/thaw cycle. Fig. 7(b) shows the individual anode polarization curve. The $|\Delta V/\Delta I|$ values suddenly increased after the 10th freeze/thaw cycle, and the polarization curves shifted along *y*-axis to the negative side. After the 10th freeze/thaw cycle, a huge amount of methanol solution was observed on the cathode side while the test block was heated at the rapidly thaw mode. Moreover, bubbles on the anode side were even more when polarization curves and EIS measurements were testing, thus, some applied air from the cathode side was supposed to penetrate the membrane. Obviously, some unexpected chemical reactions were forced to take place on the anode side, and that would make the potential abnormal. Fig. 7(c) shows the individual cathode polarization curve. The $|\Delta V/\Delta I|$ values were almost uniform before the 10th freeze/thaw cycle, but gradually increased after the 10th freeze/thaw cycle. Fig. 7(d) shows the individual membrane polarization curve. By means of the proposed measurement method, the cell voltage could be calculated by adding the voltages of the cathode and the membrane and subtracting the voltage of the anode. Because anode polarization curve shifted along *y*-axis to the negative side (Fig. 7(b)) after the 10th freeze/thaw

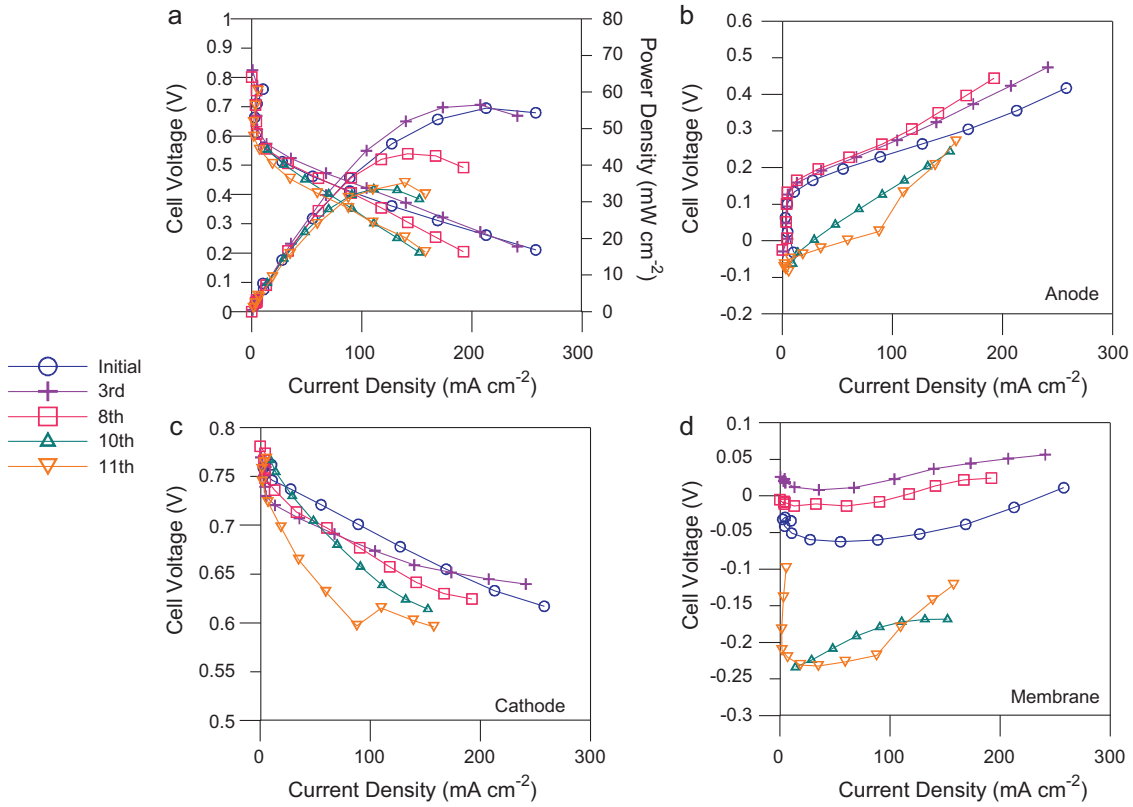

Fig. 7. Polarization curves of the MEA 3 during the freeze/thaw cycling. (a) Full-cell, (b) anode, (c) cathode, and (d) membrane. Cell temperature is 60 °C, both the anode and cathode flow are 6-stoichiometry.

cycle, thus, the membrane polarization curve presented a similar movement at the same time.

Fig. 8 shows the electrochemical behavior of the MEA 3. The 11th EIS measurement is not shown due to the dramatic degradation of the MEA 3, thus; only the first 10 data are recorded. Fig. 8(a) plots the full-cell spectrum. The HFR of the full-cell spectrum showed no significant change after the freeze/thaw cycles. Thus, the ohmic resistance of cell elements was fixed which exhibited that the MEA 3 was kept compact between the membrane, electrodes, GDLs, and other contacts. However, the CTR spectrum showed significant change during the freeze/thaw cycle. In the initial state, the CTR of the full-cell spectrum showed a small arc when the MEA 3 was in a normal condition. As the number of freeze/thaw cycles increased, the diameter of the arc gradually increased after the 3rd freeze/thaw cycle, moreover, the arc diverged in the low-frequency region after the 10th freeze/thaw cycle. The causes of the change in CTR spectra were revealed by the individual anode, cathode, and membrane impedance spectra. Fig. 8(b) presents the CTR spectrum of the individual anode. Although the diameters of arcs were almost fixed before the 10th freeze/thaw cycles, the arc became larger and diverged after the 10th freeze/thaw cycle. Fig. 8(c) presents the CTR spectrum of the individual cathode. The diameter of arc increased significantly after the 8th freeze/thaw cycle, and the arc diverged after the 10th freeze/thaw cycle. Fig. 8(d) plots the CTR spectrum of the individual membrane. Like the trend appeared on both the anode and cathode sides, the CTR spectrum on the membrane diverged suddenly after the 10th freeze/thaw cycle. Mass transport ability performed worse on the cathode side; however, it was also influenced on both the anode side and the membrane due to penetrated gas from the cathode side. Besides, the ECA values of MEA 3 shown in Fig. 9 were calculated after the 10th freeze/thaw cycle, and the values decreased 13.8% and 56.4% in the anode and cathode catalysts, respectively. However, after the 11th freeze/thaw cycle, hydrogen was perceived to cross the membrane, and that would make the reference electrode an incorrect potential. Surprisingly, after the test block was disassembled, some catalysts on the cathode side were discovered to detach from the catalyst layer. It might be the reason of huge ECA loss on the cathode side.

In summary, the $|\Delta V/\Delta I|$ value associated with the resistance R in polarization curves increased gradually as the number of freeze/thaw cycles increased on the cathode side, while those kept unchanged before the 10th freeze/thaw cycle on both the anode side and the membrane. However, the polarization curves shifted along y-axis to the negative side on both the anode side and the membrane after the 10th freeze/thaw cycle, and air crossover from the cathode side was obviously the major factor to drop the cell performance. From the CTR spectra, the mass transport problem accumulated on the cathode side, whereas the diffusion capability on the anode side and the membrane kept effective until the destructive detriment appeared after the 10th freeze/thaw cycle. The ECA results were accordant with the EIS measurements. The ECA values after the 3rd, 8th and 10th freeze/thaw cycles decreased 5.9% (not shown), 21.2% (not shown) and 56.4% in the cathode catalyst, respectively, while those decreased around only 7–15% in the anode catalyst. The detachment of catalysts on the cathode side, not only lowered the effective chemical reaction, but also added the transport resistance due to incompact microstructure.

3.4. Analysis of MEAs

As mentioned above, performance of all MEAs dropped considerably at least 35% after the freeze/thaw cycles, and the $|\Delta V/\Delta I|$ values were used to examine the individual status. Apparently, the slope of the $|\Delta V/\Delta I|$ on both the anode and cathode sides increased gradually as the number of freeze/thaw cycles increased, which

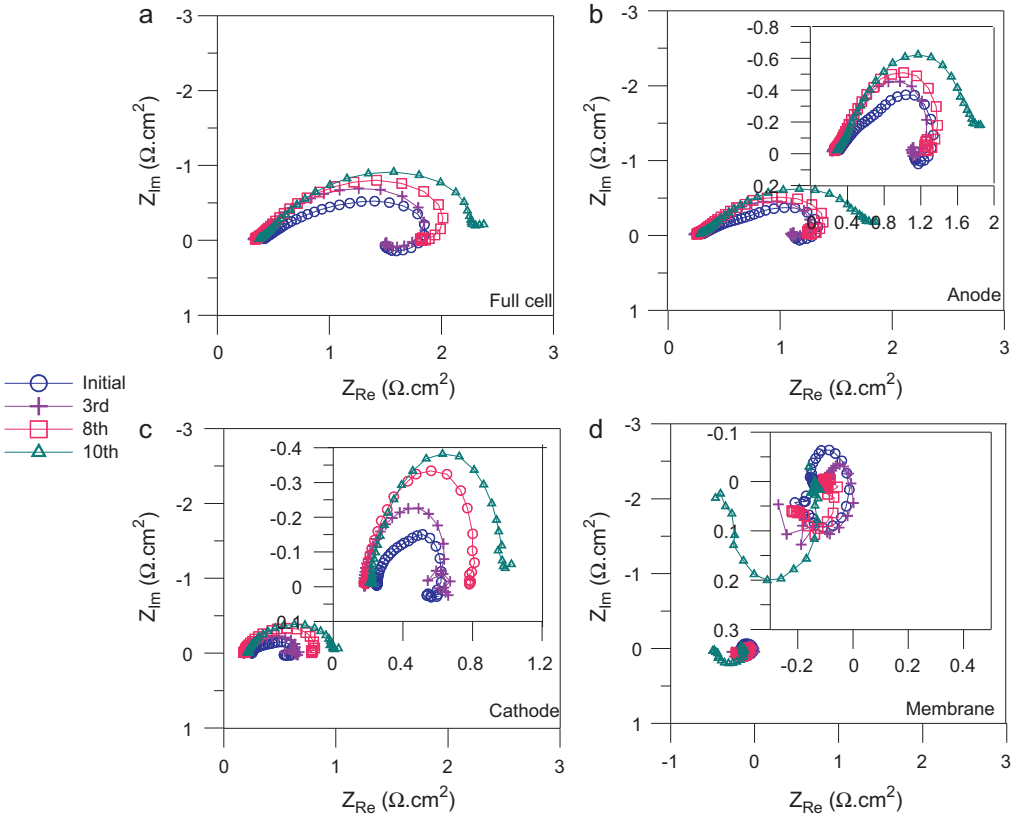

Fig. 8. EIS measurement results of the MEA 3 during the freeze/thaw cycling. (a) Full-cell, (b) anode, (c) cathode, and (d) membrane. Cell temperature is 60 °C, both the anode and cathode flow are 6-stoichiometry.

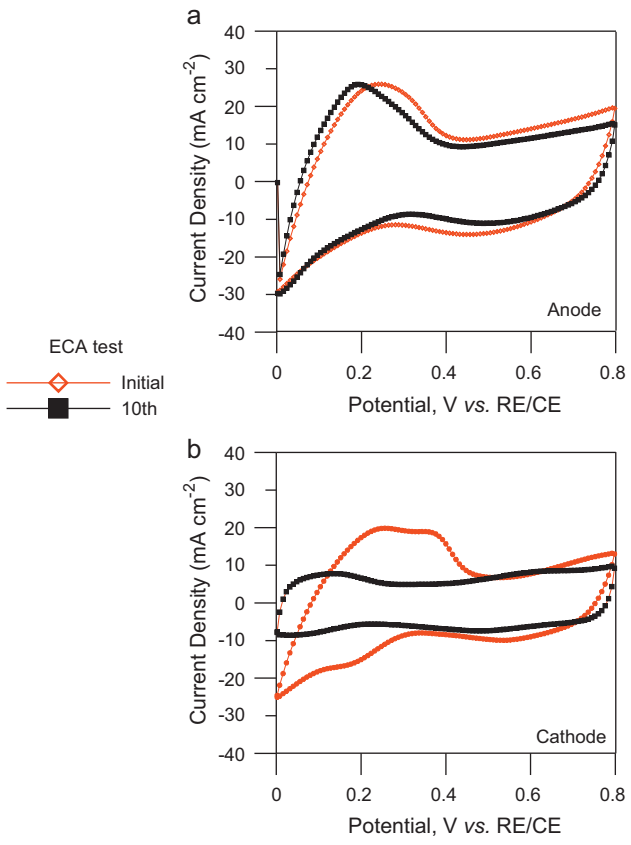

Fig. 9. Electrochemical areas (ECAs) of the catalysts on MEA 3 evaluated by hydrogen-desorption test: (a) anode catalysts and (b) cathode catalysts.

exhibited that performance loss occurred on both the anode and cathode sides, and the results were similar in all MEAs. Besides, polarization curves of the MEA 3 shifted along *y*-axis (cell voltage) to the negative side, hence, mixed potential occurred due to abnormal chemical reaction caused by penetrated air on the anode side. Certainly, formation of huge cracks in the membrane was the major contribution resulting in air crossover. Only the dominant component dropping the cell performance could be identified from the polarization curve, thus, the EIS measurement was incorporated to distinguish the degradation mechanism in detail. The HFR associated with the ohmic resistance of cell elements exhibited the sum of resistances such as the membrane, electrodes, contacts, and other components. The HFR of the MEA 1 increased after the freeze/thaw cycles due to delamination of catalyst layers and GDLs while the others did not. However, the HFR changes of the MEA 1 had less influence on cell performance since the changes were relatively small. The CTR change determined by the diameter of the arc was the key to judge the diffusion ability of the electrode. The CTR of all MEAs gradually increased on the cathode side during the freeze/thaw cycles. But, only the CTR of the MEA 1 increased on the anode side during the freeze/thaw cycles while the others kept fixed. However, the CTR of the MEA 2 and MEA 3 diverged suddenly on the anode side due to breakage of the membrane. The arc of the MEA 1 became larger and diverged on the anode side as the number of freeze/thaw cycles increased, and the double arcs from different ORR paths reflected different components of the MEA. From the CTR results, mass transport problem was more serious on the cathode side during the freeze/thaw cycles. In a PEMFC system, only the microstructure on the cathode side would be ruined due to the generated water from ORR during the freeze/thaw cycles. In a DMFC system, the anode side was full of methanol solution, but why the microstructure on the cathode side suffered much more damage? When the temperature was down to freeze point, ice would

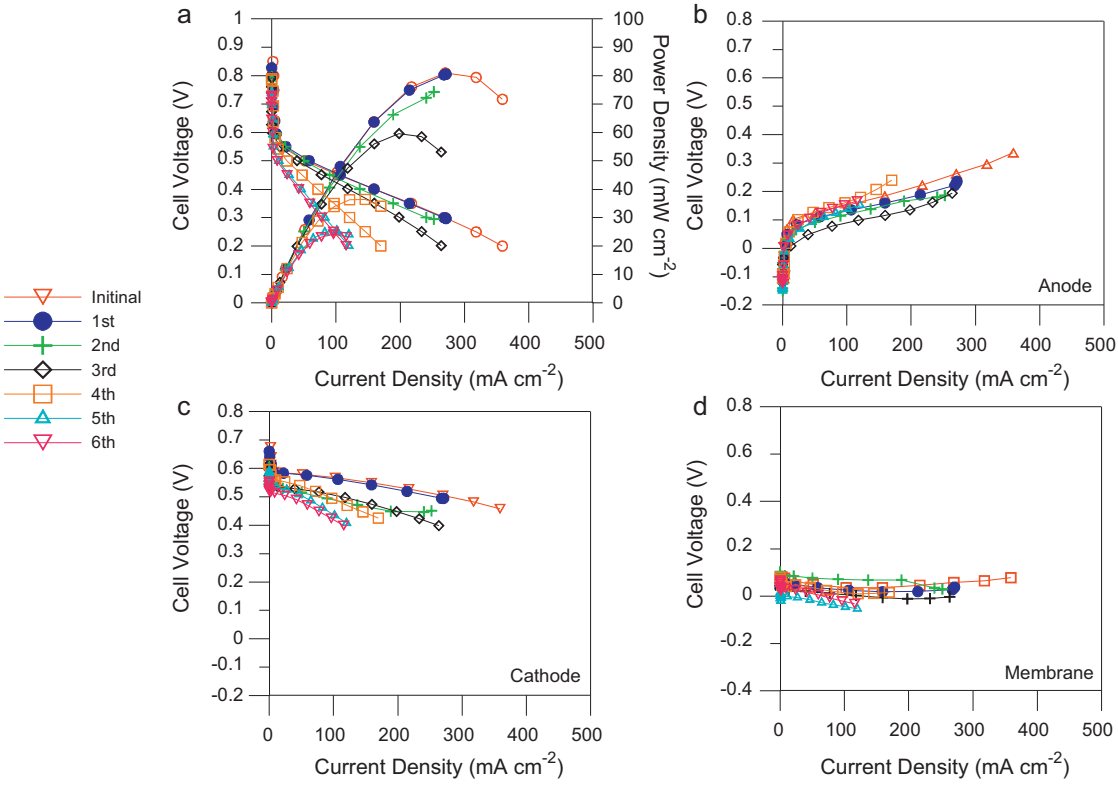

Fig. 10. Polarization curves of the real condition imposed on the MEA 2 during the freeze/thaw cycling. (a) Full-cell, (b) anode, (c) cathode, and (d) membrane. Cell temperature is 60 °C, both the anode and cathode flow are 6-stoichiometry.

form and grow in the channel, moreover, water in the anode catalyst layer would be pulled out due to the cohesion between water molecules. Fortunately, microstructure in the anode catalyst layer was prevented from being ruined during the freeze/thaw cycles. Nevertheless, water on the cathode side was accumulated in the catalyst layer. Once the ice was formed, ice in the catalyst layer would destroy the microstructure. Diffusion ability in the cathode catalyst layer was thus hindered, and the CTR was expected to increase. The anode side was full of methanol solution, and the ice produced by the freeze/thaw cycle intended to push the membrane which made the membrane more fragile. Pinholes and cracks eventually occurred, and the gas penetrated the membrane easily as the arc diverged on the anode side. From the ECA measurements, the ECA of all MEAs decreased slightly around 13-17% in the anode catalyst. During the freeze/thaw cycles, the membrane degraded gradually, once the methanol solution penetrated the membrane, the catalyst on the cathode side was poisoned immediately. The ECA loss of all MEAs in the cathode catalyst was at least 30%. Besides, the ECA loss could be convinced by the EIS measurement, as long as the CTR curve diverged due to breakage of the membrane, the ECA loss on the cathode side increased dramatically due to poison of the Pt catalyst.

3.5. Simulation of the actual condition

As mentioned above, the experiments were aborted after several freeze/thaw cycles, and breakage of the membrane was usually the major factor. In Section 3.2, the MEA 2 endured only 4 freeze/thaw cycles before huge area of hole appeared. Thus, a strategy was proposed to prevent the membrane from being broken. Before the freeze mode, a small current (0.5 A) was applied to the balance of plant (BOP) to simulate the actual shutdown condition, and the MEA 2 was chosen to implement. Fig. 10 shows the polarization curves associated with the individual anode, cathode, and membrane performance of the MEA 2. In Fig. 10(a), performance of the MEA 2 dropped about 70% after the 5th freeze/thaw cycle. Fig. 10(b) and (c) present the polarization curves of the individual anode and individual cathode, respectively. The $|\Delta V/\Delta I|$ values kept fixed on the anode side, but increased slightly on the cathode side. Besides, the individual membrane polarization curve shown in Fig. 10(d) also implied that the performance kept unchanged during the freeze/thaw cycles. It could be supposed that the performance change on the cathode side was the major cause of degraded cell performance. Fig. 11 shows the electrochemical behavior of the MEA 2. Fig. 11(a) plots the full-cell impedance spectrum. The HFR showed no significant change, therefore, the delamination of catalyst layers and GDLs could be eliminated. The arc of the CTR diverged after the 4th freeze/thaw cycle in the full-cell spectrum, and the EIS measurements of the individual anode, cathode, and membrane were incorporated to clarify the degradation mechanism. Fig. 11(b) and (c) presents the EIS spectra of the individual anode and individual cathode, respectively. The arcs became larger and diverged after the 4th freeze/thaw cycle on both the anode and the cathode side, but the CTR performed worse on the cathode side. In Fig. 11(d), however, the EIS spectrum showed no significant change during the entire freeze/thaw cycles implied the membrane was not the dominant component to influence the EIS measurement. Also, the ECA values of MEA 2 were calculated after the freeze/thaw cycles, and the values of MEA 2 decreased only 8.4% and 8.2% in the anode and cathode catalysts, respectively. The ECA loss in the cathode catalyst performed better after the strategy applied to the MEA 2, which could be explained as follow. The CO_2 bubbles on the anode side provided some space for the swelled ice, thus, the MEA 2 with less stress would prevent the membrane from being damage. Once the crossover rate decreased, the ECA loss could be suppressed. However, an unavoidable per-

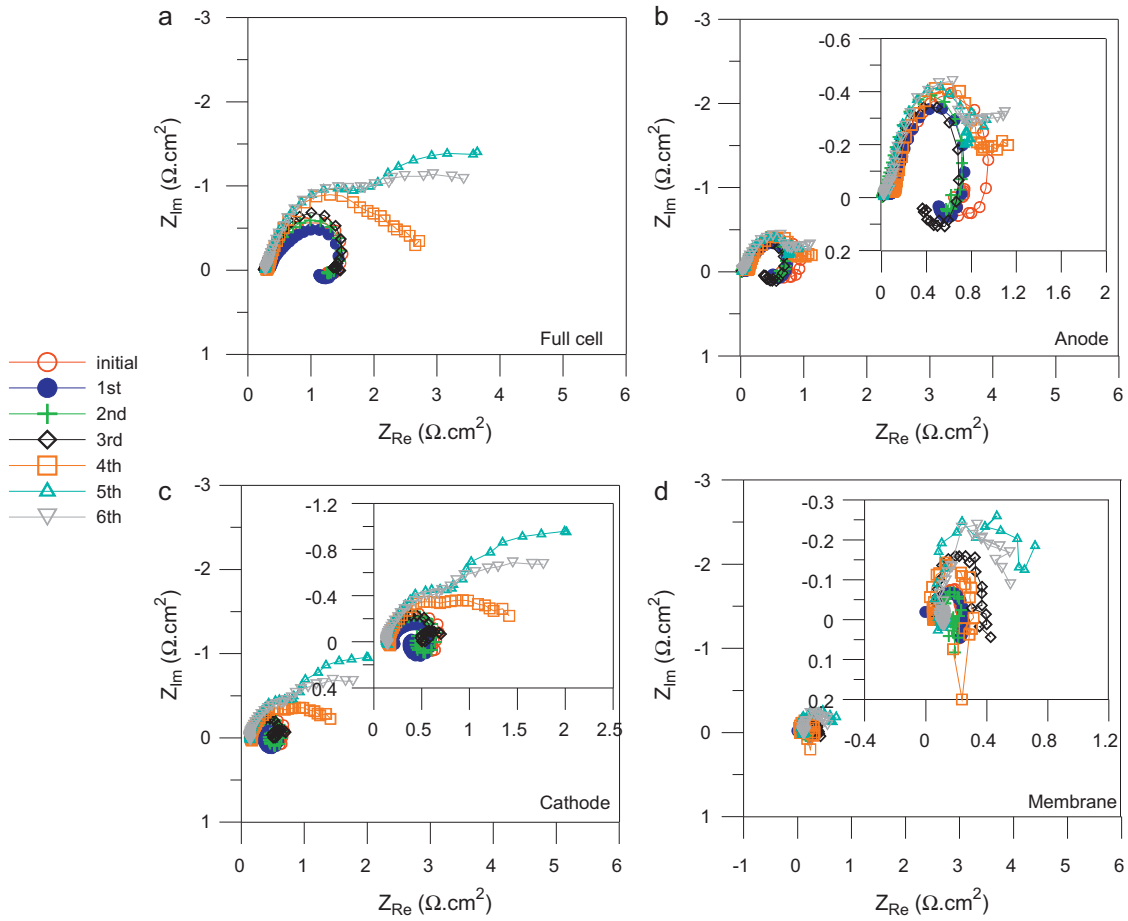

Fig. 11. EIS measurement results of the real condition imposed on the MEA 2 during the freeze/thaw cycling. (a) Full-cell, (b) anode, (c) cathode, and (d) membrane. Cell temperature is 60 °C, both the anode and cathode flow are 6-stoichiometry.

formance loss up to 70% was observed due to the microstructural damage caused by ice formation in the catalyst layer on the cathode side

4. Conclusion

This study analyzed performance and degradation in DMFC MEAs during freeze/thaw cycles. Degradation mechanisms were analyzed in three MEAs with different composition. The Ag/AgCl electrode was used as an external reference electrode to probe the individual anode, individual cathode and individual membrane during fuel cell operation. In all MEAs, cell performance degraded by at least 35% after the freeze/thaw cycles, and the dominant factor affecting the cell performance was clarified by the polarization curves, EIS measurements, and ECA results. The $|\Delta V/\Delta I|$ value associated with the resistance R was used to identify the largest effects on performance. By incorporating EIS measurements, the degradation mechanism of the MEA could be explained in detail. The ECA results not only indicated the effective chemical reaction, it also indicated the membrane condition by the sudden loss of ECA in the cathode catalyst. Notably, the microstructural damage on the cathode side was usually the major disadvantage to drop the cell performance due to the hindrance of mass transportation. The crossover phenomenon caused by the membrane defect poisoned the catalyst on the cathode side, and the experiments were eventually aborted. Although the strategy in this study was designed to prevent the membrane from being broken, the microstructure on the cathode side could not survive after the freeze/thaw cycles. Like the PEMFC system, the DMFC system sustained the microstructural damage from the ice inside the catalyst layer and GDL on the cathode side. Moreover, the catalyst of the DMFC system was poisoned after the membrane was broken. Thus, without any heating or heat-insulation devices, the methanol solution inside the DMFC stack was prevent from freezing, since, until now, no MEAs are known to be capable of withstanding the freeze/thaw cycle.

References

[1] Q. Guo, Z. Qi, J. Power Sources 160 (2006) 1269.
[2] J. Hou, B. Yi, H. Yua, L. Hao, W. Song, Y. Fu, Z. Shao, Int. J. Hydrogen Energy 32 (2007) 4503.
[3] M. Oszcipok, D. Riemann, U. Kronenwett, M. Kreideweis, M. Zedda, J. Power Sources 145 (2005) 407.
[4] M. Sundaresan, R.M. Moore, J. Power Sources 145 (2005) 534.
[5] Q. Yan, H. Toghiani, Y.-W. Lee, K. Liang, H. Causey, J. Power Sources 160 (2006) 1242.
[6] J. Hou, H. Yu, B. Yi, Y. Xiao, H. Wang, S. Sun, P. Ming, Electrochem. Solid-State Lett. 10 (1) (2007) B11.
[7] S. Ge, C.Y. Wang, Electrochim. Acta 52 (14) (2007) 4825.
[8] H. Wang, J. Hou, H. Yu, S. Sun, J. Power Sources 165 (2007) 287.
[9] U. Krewer, J.Y. Park, J.H. Lee, H. Cho, C. Pak, D.J. You, Y.H. Lee, J. Power Sources 187 (2009) 103.
[10] Y.C. Park, D.H. Peck, S.K. Kim, S. Lim, D.Y. Lee, H. Ji, D.H. Jung, Electrochem. Acta 55 (2010) 4512.
[11] J.K. Lee, J. Choi, S.J. Kang, J.M. Lee, Y. Tak, J. Lee, Electrochim. Acta 52 (2007) 2272.
[12] H. Kima, S.J. Shin, Y.G. Park, J. Song, H.T. Kim, J. Power Sources 160 (2006) 440.
[13] C.Y. Chen, P. Yang, Y.S. Lee, K.F. Lin, J. Power Sources 141 (2005) 24.
[14] C.Y. Chen, J.Y. Shiu, Y.S. Lee, J. Power Sources 159 (2006) 1042.
[15] X. Wang, J.M. Hu, I.M. Hsing, J. Electroanal. Chem. 562 (2004) 73.
[16] K.T. Jeng, C.C. Chien, N.Y. Hsu, W.M. Huang, S.D. Chiou, S.H. Lin, J. Power Sources 164 (2007) 33.
[17] C.Y. Du, T.S. Zhao, C. Xu, J. Power Sources 167 (2007) 265.
[18] J.S. Lee, K.I. Han, S.O. Park, H.N. Kim, H. Kim, Electrochim. Acta 50 (2004) 807.

[19] S.H. Yang, C.Y. Chen, W.J. Wang, J. Power Sources 195 (2010) 2319.
[20] S.H. Yang, C.Y. Chen, W.J. Wang, J. Power Sources 195 (2010) 3536.
[21] P. Piela, T.E. Springer, J. Davey, P. Zelenay, J. Phys. Chem. C 111 (2007) 6512.
[22] Z. Liu, J.S. Wainright, W. Haung, R.F. Sacinell, Electrochim. Acta 49 (2004) 923.
[23] S. Eccarius, T. Manurung, C. Ziegler, J. Electrochem. Soc. 154 (2007) B852.
[24] C.Y. Chen, C.S. Taso, Int. J. Hydrogen Energy 31 (2006) 391.
[25] H.C. Cha, C.Y. Chen, J.Y. Shiu, J. Power Sources 192 (2009) 451.
[26] S.H. Uhm, S.T. Chung, J.Y. Lee, J. Power Sources 178 (2008) 34.
[27] T.R. Ralph, G.A. Hards, J.E. Keating, S.A. Campbell, D.P. Wilkinson, M. Davis, J. St-Pierre, M.C. Johnson, J. Electrochem. Soc. 144 (1997) 3845.